Volume 7
Number 10
21 May 2023
Pages 2313–2506

Sustainable Energy & Fuels

Interdisciplinary research for the development of sustainable energy technologies

rsc.li/sustainable-energy

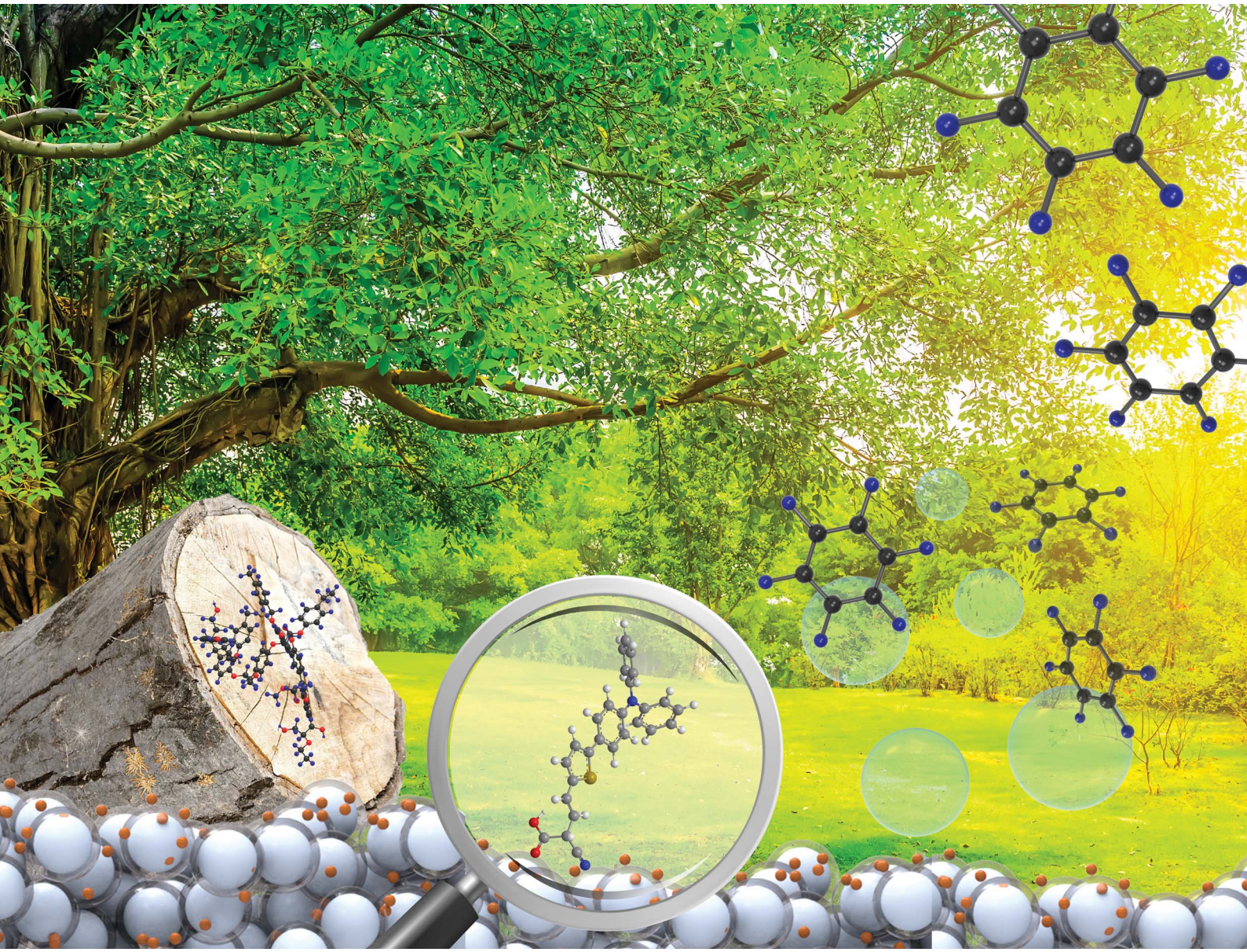

ISSN 2398-4902

ROYAL SOCIETY OF CHEMISTRY

PAPER

Jae-Joon Lee, Gyu Leem *et al.*

Solar energy driven C–C bond cleavage in a lignin model compound with a D–π–A organic dye-sensitized photoanode

Sustainable Energy & Fuels

ROYAL SOCIETY OF CHEMISTRY

PAPER

View Article Online
View Journal | View Issue

Cite this: *Sustainable Energy Fuels*, 2023, 7, 2339

Solar energy driven C–C bond cleavage in a lignin model compound with a D–π–A organic dye-sensitized photoanode†

Saerona Kim,‡[a] Hyeong Cheol Kang,‡[b] Chun Chu,[c] Shuya Li,[a] Kicheon Yoo,[b] Udani Kaushalya Wijethunga,[a] Weiwei Zheng,[c] Chang Geun Yoo,[de] Benjamin D. Sherman,[f] Jae-Joon Lee *[b] and Gyu Leem *[ae]

The high bond dissociation energy of C–C σ-bonds presents a challenge to chemical conversions in organic synthesis, polymer degradation, and biomass conversion that require chemoselective C–C bond cleavage at room temperature. Dye-sensitized photoelectrochemical cells (DSPECs) incorporating molecular organic dyes could offer a means of using renewable solar energy to drive these types of energetically demanding chemoselective C–C bond cleavage reactions. This study reports the solar light-driven activation of a bicyclic aminoxyl mediator to achieve C–C bond cleavage in the aryl-ether linkage of a lignin model compound (**LMC**) at room temperature using a donor–π-conjugated bridge–acceptor (D–π–A) organic dye-based DSPEC system. Mesoporous TiO_2 photoanode surfaces modified with 5-[4-(diphenylamino)phenyl]thiophene-2-cyanoacrylic acid (**DPTC**) D–π–A organic dye were investigated along with a bicyclic aminoxyl radical mediator (9-azabicyclo[3,3,1]nonan-3-one-9-oxyl, **KABNO**) in solution with and without the presence of **LMC**. Photophysical studies of **DPTC** with **KABNO** showed intermolecular energy/electron transfer under 1 sun illumination (100 mW cm^{-2}). Under illumination, the D–π–A type **DPTC** sensitized TiO_2 photoanodes facilitate the generation of the reactive oxoammonium species $KABNO^+$ as a strong oxidizing agent, which is required to drive the oxidative C–C bond cleavage of **LMC**. The photoelectrochemical oxidative reaction in a complete DSPEC with **KABNO** afforded C–C bond cleavage products 2-(2-methoxyphenoxy)acrylaldehyde (94%) and 2,6-dimethoxy-1,4-benzoquinone (66%). This process provides a first report utilizing a D–π–A type organic dye in combination with a bicyclic nitroxyl radical mediator for heterogeneous photoelectrolytic oxidative cleavage of C–C σ-bonds, modeled on those found in lignin, at room temperature.

Received 15th February 2023
Accepted 16th March 2023

DOI: 10.1039/d3se00194f

rsc.li/sustainable-energy

Introduction

Lignin is one of the most abundant natural aromatic resources on Earth and is recognized as a potential feedstock for alternative fuels and chemicals.[1] Lignin valorization requires a cost effective means of driving the energy intensive conversion of lignin to value-added monomeric chemicals (*e.g.*, vanillin, catechol, and phenol) that are important raw materials for the production of bioplastics, adhesives, and pharmaceuticals.[2–9] In addition, lignin is reported as a precursor for a polymeric composite that can be used for various energy applications.[10–13] Phenolic aromatic units are abundant in lignin and connected by aliphatic C–C and/or C–O σ-bonds, which are the targeted linkages for most lignin degradation strategies (Fig. 1a).[14] In the past few years, C–C and/or C–O bond cleavages in lignin model compounds or real lignin have been performed using various reaction methods including retro-aldol reaction,[2,15] catalytic aerobic oxidation,[3,4,14,16,17] hydrogenation,[5] **TEMPO**-mediated oxidation (**TEMPO** = 2,2,6,6-tetramethyl-1-piperidine *N*-oxyl),[6] electrocatalytic oxidation,[7] and photocatalytic oxidation/reduction.[8,18] Among these, we first reported the photoelectrocatalytic oxidation of lignin model compounds and real lignin using a polypyridyl based Ru(II) complex chromophore coated mesoporous TiO_2 photoanode with a hydrogen atom transfer mediator (*e.g.*, *N*-hydroxyphthalimide) in a dye-sensitized

[a]*Department of Chemistry, State University of New York College of Environmental Science and Forestry, Syracuse 13210, New York, USA. E-mail: gyleem@esf.edu*

[b]*Department of Energy and Materials Engineering, Research Center for Photoenergy Harvesting & Conversion Technology (phct), Dongguk University, Seoul 04620, Republic of Korea. E-mail: jjlee@dongguk.edu*

[c]*Department of Chemistry, Syracuse University, Syracuse 13244, New York, USA*

[d]*Department of Chemical Engineering, State University of New York College of Environmental Science and Forestry, Syracuse 13210, New York, USA*

[e]*The Michael M. Szwarc Polymer Research Institute, 1 Forestry Drive, Syracuse 13210, New York, USA*

[f]*Department of Chemistry and Biochemistry, College of Science and Engineering, Texas Christian University, Fort Worth 76129, Texas, USA*

† Electronic supplementary information (ESI) available: Details of additional characterization methods and data. See DOI: https://doi.org/10.1039/d3se00194f

‡ S. K. and H. C. K. are equally contributed to this paper.

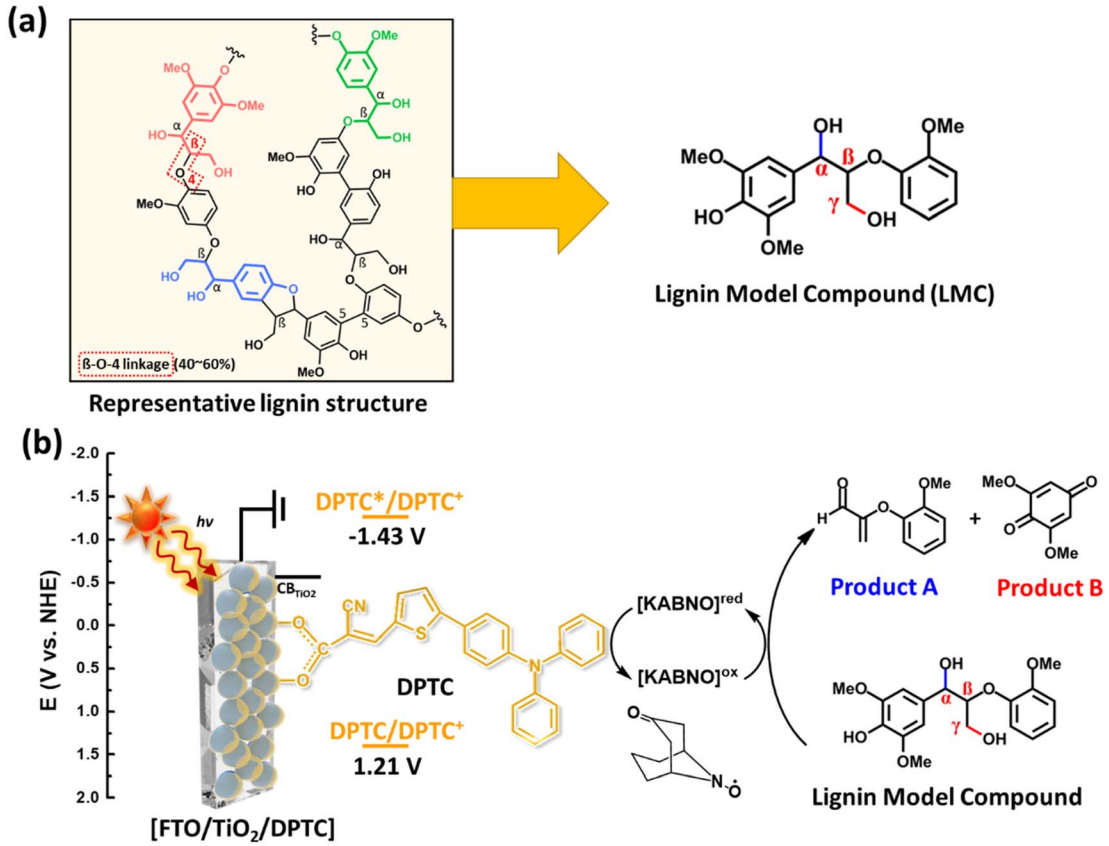

Fig. 1 (a) Schematic representative structure of real lignin (left) and a dimeric lignin model compound (LMC) containing abundant aryl ether linkage (right), and (b) illustration of DPTC anchored on mesoporous structured TiO_2 for solar light-driven oxidative cleavage of LMC in combination with a bicyclic nitroxyl mediator, 9-azabicyclo[3,3,1]nonan-3-one-9-oxyl (KABNO).

photoelectrochemical cell (DSPEC) under solar light illumination at room temperature.[19] Traditionally, DSPECs have targeted solar-driven water oxidation/reduction for the production of solar fuels in aqueous media.[20–22] Notably, Ru polypyridyl complexes have been extensively studied with co-catalysts for water oxidation or reduction reactions, solar energy conversion, and solar fuel production.[23–25] However, these Ru based complexes share the drawback of high materials cost and the limited ability to tune the HOMO and LUMO energy levels as compared to organic dyes.[26] Metal-free organic dyes containing a donor–π-conjugated bridge–acceptor (D–π–A) structure offer promising alternatives as the photocatalyst for the light-driven oxidative C–C bond cleavage of lignin in the DSPEC system because of their high molar absorption coefficient, tunable redox potentials, and facile synthesis.[27] To our knowledge, oxidative cleavage of C–C bond in lignin or related model compounds in a DSPEC at room temperature has not been explored to date using D–π–A type organic chromophores.

Direct electrochemical oxidative C–O and/or C–C bonds cleavage of lignin model species has been widely studied.[28–30] However, this approach requires high applied bias to deliver sufficient overpotential (*e.g.*, 1.45 V *vs.* SCE) resulting in the formation of unwanted oxidation and degradation products.[31] Electrolysis in the presence of a nitroxyl mediator (*e.g.*, **TEMPO**) provides an alternative approach that lowers by several hundred mV the required overpotential compared with the direct oxidation of the lignin model compound or real lignin degradation.[32,33] For example, the Stahl research group found that monocyclic **TEMPO** and its derivatives facilitated the oxidation of secondary benzylic alcohol or aliphatic primary alcohol groups in lignin under sufficient electrochemical bias.[34] In addition, the use of bicyclic nitroxyls (*e.g.*, 2-azaadamantane *N*-oxyl and **KABNO**) showed significant oxidation activity for primary and/or secondary alcohol oxidation due to their favorable catalytic properties.[35–37] However, bicyclic nitroxyls species have not been as extensively studied in a DSPEC system even though they have been known as effective alcohol oxidation agents since the 1960s.[35,38] To complement these dark electrochemical and electrocatalytic approaches, our study presents the next step in lowering the electrical energy (*e.g.*, < 0.5 V *vs.* Ag/Ag^+) needed to achieve chemoselective C–C bond cleavage of lignin by harnessing solar energy at room temperature using an organic dye-based DSPEC incorporating a bicyclic nitroxyl mediator. As shown in Fig. 1b, this article describes the use of D–π–A type organic dye-sensitized TiO_2 photoanodes in combination with a bicyclic nitroxyl mediator, 9-azabicyclo [3,3,1]nonan-3-one-9-oxyl (**KABNO**), to carry out C–C bond cleavage of aryl-ether linkages in a phenolic lignin model compound (**LMC**) under simulated solar illumination at room temperature. The 5-[4-(diphenylamino)phenyl]thiophene-2-

cyanoacrylic acid (**DPTC**) D–π–A organic dye featuring a triphenylamine (TPA) donor, cyanoacrylic acceptor moiety, and carboxylic anchoring group was chosen as a typical D–π–A typed dye, which is widely used in dye-sensitized solar cells because of its high molar extinction coefficients in the visible range.[39] In addition, the redox potential of **KABNO** is a good match for the HOMO level of **DPTC** as shown in Fig. 1b. The **KABNO**$^{\bullet/+}$ couple exhibits a relatively high redox potential compared to other *N*-oxyl species of 200 mV *vs.* Fc^+/Fc in acetonitrile with 0.1 M $LiClO_4$.[40] Fig. 1b gives a schematic overview of the solar-light-driven selective C–C bond cleavage process studied here involving 1-(4-hydroxy-3,5-dimethoxyphenyl)-2-(2-methoxyphenoxy)propane-1,3-diol as the **LMC**, the **DPTC**-sensitized TiO_2 photoanode (FTO/TiO_2/DPTC), and solution dissolved **KABNO** under 1 sun illumination. This phenolic **LMC** structure contains the most abundant aryl ether linkage type found in native lignin.

Experimental section

Materials

5-[4-(Diphenylamino)phenyl]thiophene-2-cyanoacrylic acid was purchased from Dyenamo. Fluorine-doped tin oxide glass was purchased from Hartford Glass Co., Inc. Tetrabutylammonium hexafluorophosphate ($TBAPF_6$) was purchased from TCI. 9-Azabicyclo[3,3,1]nonan-3-one-9-oxyl was purchased from Sigma-Aldrich. The **LMC**, 1-(4-hydroxy-3,5-dimethoxyphenyl)-2-(2-methoxyphenoxy)propane-1,3-diol, was purchased from SY Innovation and used without further purification or modification.

Fabrication of DPTC-immobilized mesoporous TiO_2 photoanode (FTO/TiO_2/DPTC)

The photoanodes were fabricated and modified according to previous studies.[19,41,42] All FTO glass was cleaned by sonicating it with detergent, distilled water, and the mixture of acetone, isopropyl alcohol, and ethanol (1 : 1 : 1 ratio), separately, in an ultrasonic bath for 20 min. The mesoporous structured TiO_2 layer was prepared by doctor blading a TiO_2 paste (approximately 20 nm TiO_2) onto a clean FTO glass slide followed by annealing at 500 °C for 30 min.[43–45] Then, after cooling down to 80 °C, the annealed TiO_2 films (FTO/TiO_2) were immersed in a 0.5 mM **DPTC** solution in anhydrous ethanol for 4 h at room temperature. The FTO/TiO_2/DPTC films were rinsed with anhydrous ethanol, dried, and stored in a sealed vial prior to use.

Characterization methods

UV-visible absorption spectra of FTO/TiO_2/DPTC films were collected using a Thermo Scientific Evolution 220 UV-vis spectrometer. Emission spectra measurement was performed using an Edinburgh FLS 980 steady state fluorometer. The AFM images of bare FTO/TiO_2 and FTO/TiO_2/DPTC films were obtained with tapping mode of 0.7 Hz using the MultiMode-8 and RTESP-300 tip (Bruker Co.). All cleavage products were characterized by NMR, GC-FID (Shimadzu 2010 GC), and GC-MS (Q Exactive GC Orbitrap GC-MS/MS with TriPlus RSH autosampler). ^{1}H-NMR, ^{13}C-NMR, and 2D ^{1}H–^{13}C heteronuclear single quantum coherence (HSQC) NMR were used for the structural analysis of **LMC** before and after photoelectrochemical reaction by using a Bruker AVANCE III HD 800 MHz equipped with TCI Cryo probe. The HSQC NMR spectra were processed using Bruker TopSpin 4.1.4 software. After the completion of the reaction, all reaction mixtures were precipitated by a 1 : 1 mixture of ethyl acetate and hexane to remove the $TBAPF_6$ electrolyte. Then, the products were dissolved in $CDCl_3$ with dimethyl sulfoxide (DMSO) as an internal standard for NMR analysis. The conversion yield of the cleavage products was obtained by GC-FID fitted with a 30 m × 0.25 mm i.d. capillary column and AOCI205 autosampler. Helium gas was used as a carrier gas and the GC-FID system was held at 65 °C for 3 min. The temperature was ramped from 65 to 300 °C with a heating rate of 10 °C min^{-1}, and kept at 300 °C for 5 min. The concentration of each product was determined based on the product calibration curve with the internal standard DMSO. The cleavage products were confirmed by GC-MS. The GC-MS system was held at 40 °C for 3 min, and then the temperature was gradually increased from 40 to 300 °C with a heating rate of 10 °C min^{-1}, and then held at 300 °C for 20 min.

Electrochemical measurements

All electrochemical measurements were performed in acetonitrile solution with 0.1 M $TBAPF_6$ as a supporting electrolyte using a single compartment three-electrode cell including a Pt wire counter electrode, a Ag/Ag^+ quasi reference electrode, and FTO/TiO_2/DPTC films as the working electrode. Voltammograms were recorded at a scan rate of 50 mV s^{-1} and potentials were reported with ferrocene/ferrocenium (Fc/Fc^+) as an external reference after calibration of the Ag/Ag^+ quasi reference. Photocurrent-time trace measurements were conducted at light intervals of 60 s on/off with an applied voltage of +0.4 V *vs.* Ag/Ag^+ under 1 sun illumination (100 mW cm^{-2}). Light irradiation was provided by an AM1.5 solar simulator (Abet Technologies). The temperature in the photoanode was maintained at ambient temperature by cooling with forced air using an electric fan.

Photoelectrocatalytic oxidation of LMC

All lignin model compound (**LMC**) degradation studies were performed using an LSH-7320 ABA LED Solar Simulator (ORIEL) with 1 sun AM1.5 G (100 mW cm^{-2}) light intensity for 24 hours under an applied voltage of +0.4 V *vs.* Ag/Ag^+. The light intensity was measured using a THORLABS PM400 optical power meter with a S415C thermal power sensor head. The electrolyte solution contained 3 mM **KABNO** and 8 mM **LMC** in 20 mL of acetonitrile with 0.1 M $TBAPF_6$. A specifically designed Teflon cell suitable for back-illumination was used to assemble all the organic dye-sensitized DSPECs.

Results and discussion

The photophysical properties of **DPTC** were studied in the presence or absence of **KABNO** in acetonitrile solution. The UV-

visible absorption and emission spectra of **DPTC** show a broad absorption and emission with peak maximum at $\lambda \approx 385$ and 525 nm, respectively (Fig. 2a). It is noted that the absorption approximately between 380 to 500 nm corresponds to the charge transfer from the triphenylamine donor to the cyanoacrylic acid acceptor unit.[46,47] The steady-state emission intensity of **DPTC** decreases as the concentration of **KABNO** increases from 0 to 1.2 mM (Fig. 2b), which indicates that the emission from the photoexcited **DPTC** was quenched by the presence of **KABNO**. On the basis of emission quenching in Fig. 2b, the Stern–Volmer quenching constant value obtained approximately $K_{sv} \sim 5.5 \times 10^2$ M^{-1}. This emission quenching implies that intermolecular energy/electron transfer between the photoexcited **DPTC** and **KABNO** occurs. This could result in the formation of oxidized **KABNO**$^+$ following photoexcited charge transfer between **DPTC*** and **KABNO**.[48] On the basis of this quenching, we expect that photoexcited electron from **DPTC*** is injected into the TiO_2 photoanode generating **DPTC**$^+$ which then drives the formation of oxoammonium **KABNO**$^+$ by interfacial hole transfer in the DSPEC.

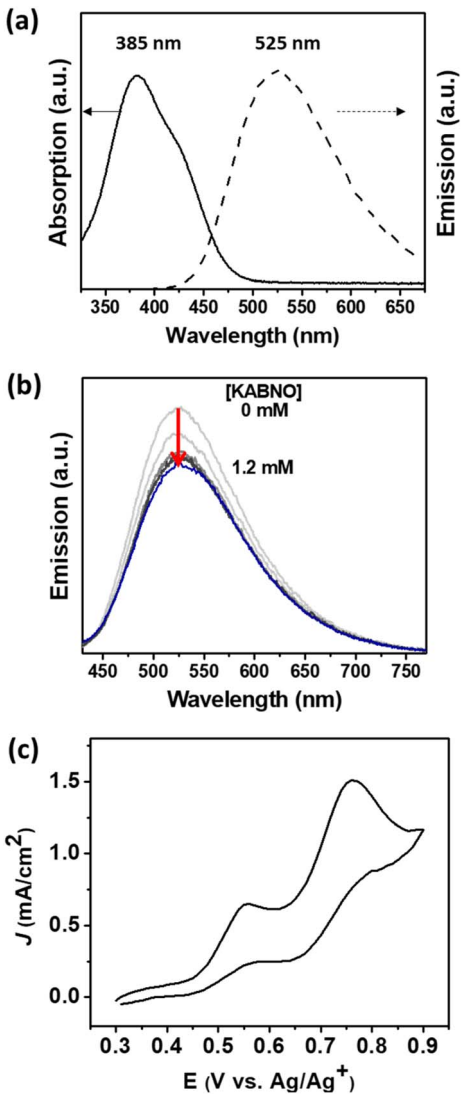

Fig. 2 (a) UV-vis absorption (solid) and emission (dash) spectra of DPTC in acetonitrile. Emission spectrum was obtained with excitation at $\lambda_{ex} = 380$ nm. (b) Emission quenching for DPTC with KABNO (conc. = 0–1.2 mM). (c) CV of KABNO and LMC in 0.1 M $TBAPF_6$ acetonitrile solution. The experiment was performed using a glassy carbon working electrode, Pt counter electrode, and Ag/Ag^+ reference electrode in the dark.

Cyclic voltammetry (CV) was carried out in acetonitrile to study the relative redox potentials of **KABNO** and **LMC** using a glassy carbon working electrode. **KABNO** showed stable redox behavior with $E_{1/2} = 0.54$ V *vs.* Ag/Ag^+ (Fig. S1a†); however, an irreversible anodic wave was observed for **LMC** with $E_{pa} = 0.76$ V *vs.* Ag/Ag^+ (Fig. S1b†) which is consistent with other studies.[31,49] The addition of 3 mM of **LMC** to the **KABNO** solution results in both increased current at the anodic peak of the **KABNO** wave ($E_{pa} = 0.56$ V *vs.* Ag/Ag^+, Fig. 2c) and the loss of the cathodic wave for **KABNO** on the return scan. Both observations are consistent with the catalytic oxidation of **LMC** by **KABNO**$^+$ in solution after its formation by interfacial electron transfer.[31,32,37,50,51] These results reveal that **KABNO**$^+$ can effectively oxidize the alcohol groups in **LMC**, and it demonstrates the importance of nitroxyl mediators (*i.e.*, **KABNO**) in lowering the activation energy for converting the **LMC** to the corresponding ketone/aldehyde as reported in previous studies.[52]

To fabricate a **DPTC**-sensitized photoanode, mesoporous TiO_2 films with a thickness of ~6 μm were deposited on FTO substrates.[42] The **DPTC** dye was adsorbed onto the FTO/TiO_2 films (FTO/TiO_2/DPTC) from 0.5 mM ethanol solution at room temperature. Fig. 3a shows the absorption spectrum with $\lambda_{max} \approx 410$ nm of the FTO/TiO_2/DPTC surface corresponds to the charge transfer from a TPA donor to cyanoacrylic acceptor unit. This maximum absorption band of **DPTC** at the interface of the FTO/TiO_2 film displays a similar absorption band with ~420 nm in ethanol solution (Fig. S2†). This absorption band is shifted to a shorter wavelength (*i.e.*, blue-shift) compared to **DPTC** in ethanol solution due to the adsorption on the TiO_2 surface.[19] The plane view topographies of the bare FTO/TiO_2 and FTO/TiO_2/DPTC films were further characterized by atomic force microscopy (AFM) (Fig. S3†). AFM analysis of the FTO/TiO_2/DPTC films revealed a smoother surface with roughness, $R_{rms} = 24$ nm (R_{rms}: root mean square), compared to that of the FTO/TiO_2 films ($R_{rms} = 28$ nm). These results indicate that the **DPTC** dye is successfully anchored onto the TiO_2 surface.

To investigate the electrochemical response of FTO/TiO_2/DPTC films in the absence or presence of **KABNO** and **LMC**, CVs were performed in 0.1 M $TBAPF_6$ acetonitrile solution, as shown in Fig. 3b. The CV of FTO/TiO_2/DPTC exhibits steady redox behavior, with a redox couple at $E_{1/2} = 0.76$ V *vs.* Ag/Ag^+ (black voltammogram). In the presence of **KABNO**, the voltammogram shows corresponding redox potential peaks at $E_{1/2} = 0.50$ V *vs.* Ag/Ag^+ (blue voltammogram), while the mixture of **KABNO** and **LMC** in acetonitrile solution exhibits increased anodic current at a high applied bias > 1.2 V *vs.* Ag/Ag^+ (red voltammogram). The increase in peak current for the **KABNO** anodic wave in the red voltammogram and the absence of cathodic peaks for **KABNO** and **DPTC** on the return scan are consistent with the oxidizing equivalents generated ultimately resulting in the oxidation of **LMC**.[52] In other words, the formation of **KABNO**$^+$

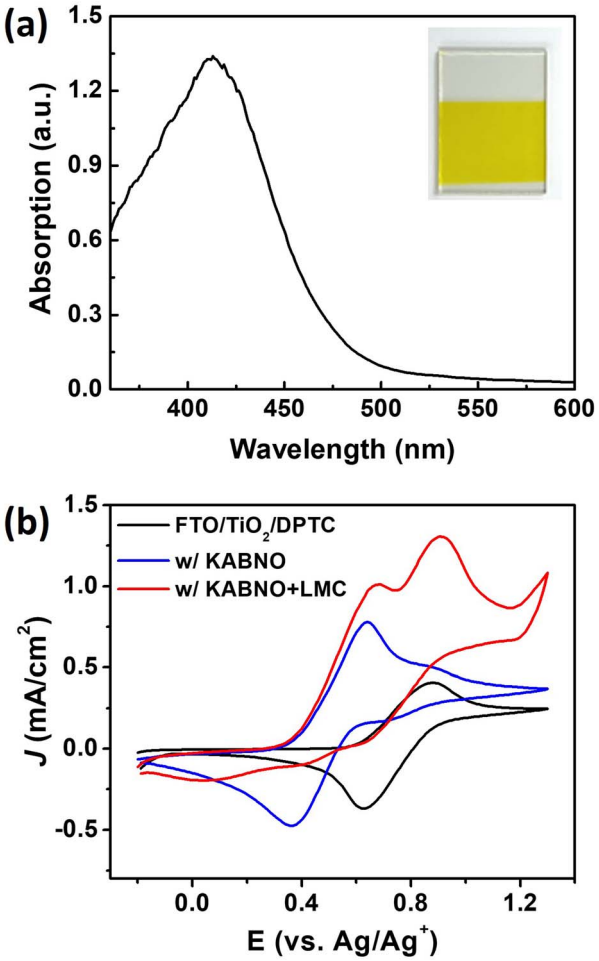

Fig. 3 (a) UV-vis spectrum of FTO/TiO_2/DPTC (inset: picture of a FTO/TiO_2/DPTC electrode). (b) CVs of FTO/TiO_2/DPTC (black), the same with 3 mM **KABNO** (blue), and the mixture of 3 mM **KABNO** and **LMC** (red) in 0.1 M $TBAPF_6$ acetonitrile.

occurs at 0.64 V *vs.* Ag/Ag^+; however, the cathodic peak for the reduction of **KABNO**$^+$ back to **KABNO** expected at 0.37 V *vs.* Ag/Ag^+ does not appear because of the reaction of **KABNO**$^+$ with **LMC** in solution. As a control experiment and for further comparison, a CV of the FTO/TiO_2/DPTC film was performed with only **LMC** in solution as shown in Fig. S4.†

The photocurrent transient experiments with FTO/TiO_2/DPTC in the presence of **KABNO** and/or **LMC** in solution are shown in Fig. 4. Increasing the **KABNO** concentration from 0, 1.5, 3.0, to 5.0 mM in 0.1 M $TBAPF_6$ acetonitrile solution resulted in increasing photocurrent densities of 10, 53, 133, and 197 μA cm^{-2}, respectively (Fig. 4a). The increased photocurrents with increasing [**KABNO**] suggest that light-driven electron transfer from **KABNO** to oxidized **DPTC**$^+$ dye occurs following charge injection from **DPTC*** to the conduction band of mesoporous TiO_2. According to the photocurrent experiments, the total consumed charge passed during the photocurrent measurements showed 1.5, 5.8, 14.9, and 19.7 mC with increasing [**KABNO**] of 0, 1.5, 3.0, and 5.0 mM **KABNO**, respectively (Fig. 4b). The linear increase in charge passed shows that **DPTC** dye is capable of generating the activated **KABNO**$^+$ as a strong oxidizing mediator for lignin oxidation under visible light illumination. To probe **LMC** oxidation in this DSPEC system, 3 mM of **LMC** was added to the solution in the presence of **KABNO** under the same photoelectrochemical conditions. Interestingly, the photocurrent significantly increased up to ~603 μA cm^{-2} (Fig. 4c). As a control experiment, the photocurrent was measured for FTO/TiO_2/DPTC with 3 mM **LMC** and no **KABNO** (Fig. S5†). With **LMC** in solution, the photocurrents do increase compared to blank electrolyte (no **LMC** and **KABNO**). The lower observed photocurrent (~210 μA cm^{-2}) with only 3 mM **LMC** in solution compared to that of the mixture of **LMC** and **KABNO** (603 μA cm^{-2}) demonstrates that the maximum photocatalytic activity requires the presence of both **LMC** and **KABNO**. The substantial increase in photocurrent is attributed to the effective oxidation of **LMC** by the oxoammonium species **KABNO**$^+$ generated at the FTO/TiO_2/DPTC surface under 1 sun illumination. Interestingly, reproducible current spikes are observed in the first 30 s of illumination in the presence of both **KABNO** and **LMC**. To gain further insight into transient spikes in Fig. 4c, we performed additional experiments with varying concentration of **KABNO** to understand better the conditions that cause the current spikes. In Fig. 4d, the **KABNO** concentration is varied from 1.5 to 6.0 mM while [**LMC**] is constant. Fig. 4e shows a magnified view of the photocurrents between 5 and 6 min. Based on these observations, the transient photocurrent peaks appear when the **LMC** concentration is the same or higher than [**KABNO**]. Upon close inspection of the current spike at the 6.0 mM **KABNO** condition (blue), a growth in photocurrent is still observed following the start of illumination, but peaks at a shorter time (~5 s) after the start of illumination. As shown in Fig. 4e, the photocurrent transients can be characterized by four stages: (I) photocurrent onset and initial decay, (II) delayed increase in photocurrent reaching a peak, (III) a second decay period following the peak, and (IV) steady state photocurrent at longer (>30 s) illumination times. While these states are most obvious in the 1.5 mM and 3.0 mM experiments (black and red), the 6.0 mM **KABNO** (blue) shows similar behavior but with shorter periods for each stage. We interpret the behavior of the photocurrent in each stage as reflective of the reductants present in the double layer. Initially (stage I), only **KABNO** is present and the photocurrent decays as a diffusional gradient establishes under illumination. As the concentration of oxoammonium increases from the oxidation of **KABNO**, the reaction with **LMC** produces reductants not initially present either by the generation of **KABNOH** or the intermediates formed after reaction of the **LMC** with **KABNO**$^+$. This increase in reductant concentration in the double layer as a result of chemical reaction of the photochemically generated **KABNO**$^+$ causes an increase in the photocurrents (stage II) that peak and gradually decline as all the **LMC** in the double layer is consumed (stage III). After sufficient time (stage IV), diffusional gradients of **KABNO** and **LMC** establish and the system reaches a steady state that, in the presence of equal or greater concentration of **KABNO**, depends on the bulk concentration of **LMC** (compare 3.0 mM (red) and 6.0 mM (blue) data sets in Fig. 4e).

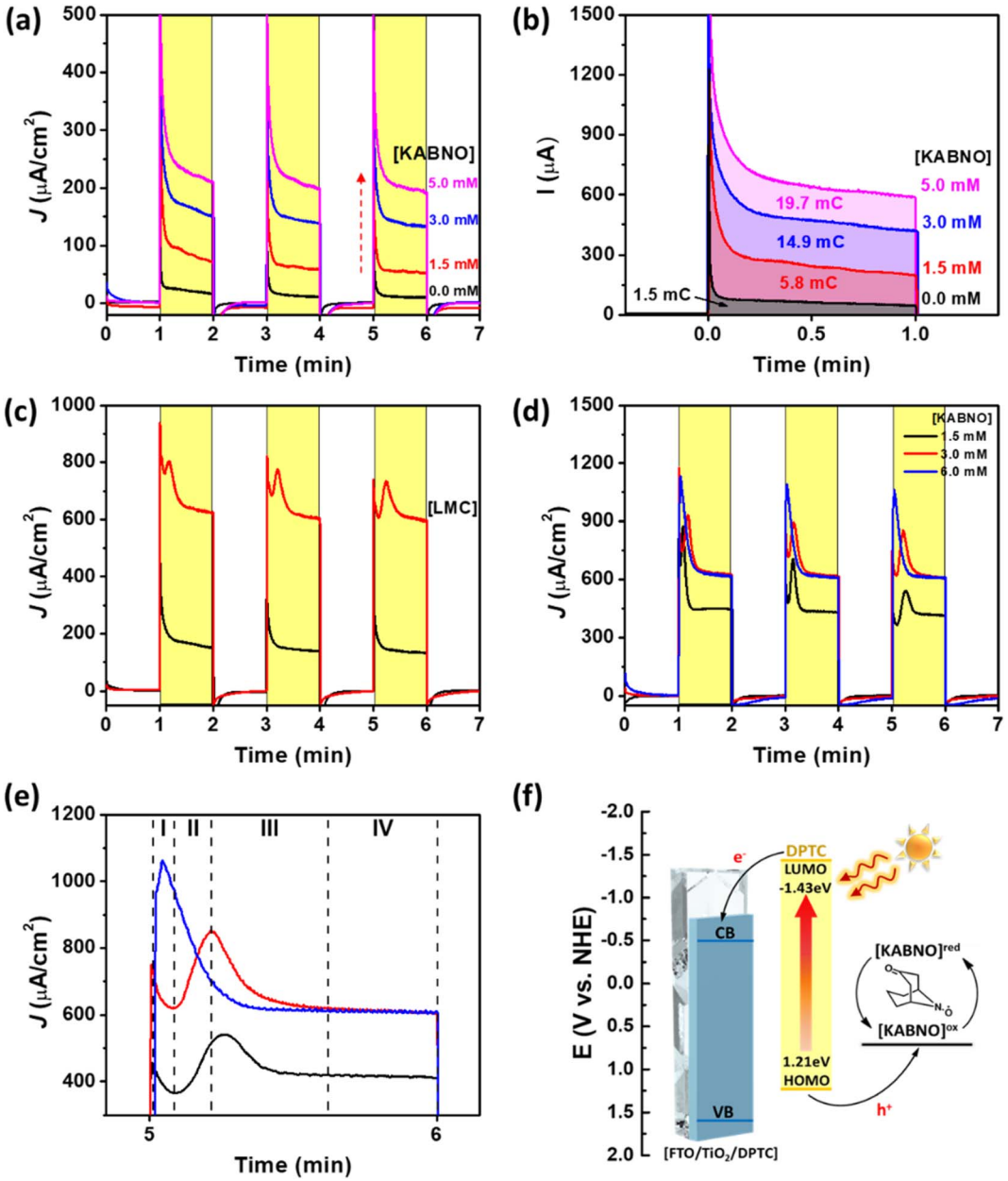

Fig. 4 (a) Photocurrent-time trace of FTO/TiO_2/DPTC (black) with different concentration of **KABNO** (red: 1.5 mM, blue: 3.0 mM, and pink: 5.0 mM). (b) Chronoamperograms of the FTO/TiO_2/DPTC electrode in the presence of increasing concentration of **KABNO** from under illumination from time 0 to 1 min. Photocurrent-time trace of FTO/TiO_2/DPTC (c) with 3 mM **KABNO** (black) and the mixture of 3 mM **KABNO** and **LMC** (red), (d) with different concentration of **KABNO** (black: 1.5 mM, red: 3.0 mM, and blue: 6.0 mM) at 3 mM **LMC**, and (e) the photocurrent densities with the period of between 5 and 6 min. (f) Energy diagram of the mesoporous TiO_2, **DPTC**, and **KABNO** components of system. CB and VB indicate the conduction band and valence band potential of TiO_2, respectively. All photocurrent-time trace experiments performed in 0.1 M $TBAPF_6$ acetonitrile solution with an applied bias of 0.4 V *vs.* Ag/Ag^+ under 1 sun illumination.

While the number of *N*-oxyl species near the electrode is constant, the reaction of one equivalent **KABNOH** (R_2NOH) at the electrode to give **KABNO**$^+$ delivers two electron equivalents. Only **KABNO** should be present at the start of illumination, and the formation of some amount of **KABNOH** as a result of reactions in solution with **LMC** and **KABNO**$^+$, and then the oxidation of **KABNOH** to **KABNO**$^+$ at the photoanode, could explain the growth in photocurrent immediately following the start of illumination. Taken together, these results demonstrate the effective photoelectrochemical transformation of **LMC** proceeding by the following steps: (i) light absorption and photoexcited electron injection from **DPTC*** to the conduction band of TiO_2, (ii) hole transfer between oxidized **DPTC**$^+$ and **KABNO** to form the oxoammonium species **KABNO**$^+$ in solution, (iii) oxidation of **LMC** by **KABNO**$^+$ ($[KABNO]^{ox}$), and (iv) regeneration of **KABNO** ($[KABNO]^{red}$ Fig. 4f) and the C–C cleaved products **A** and **B**.

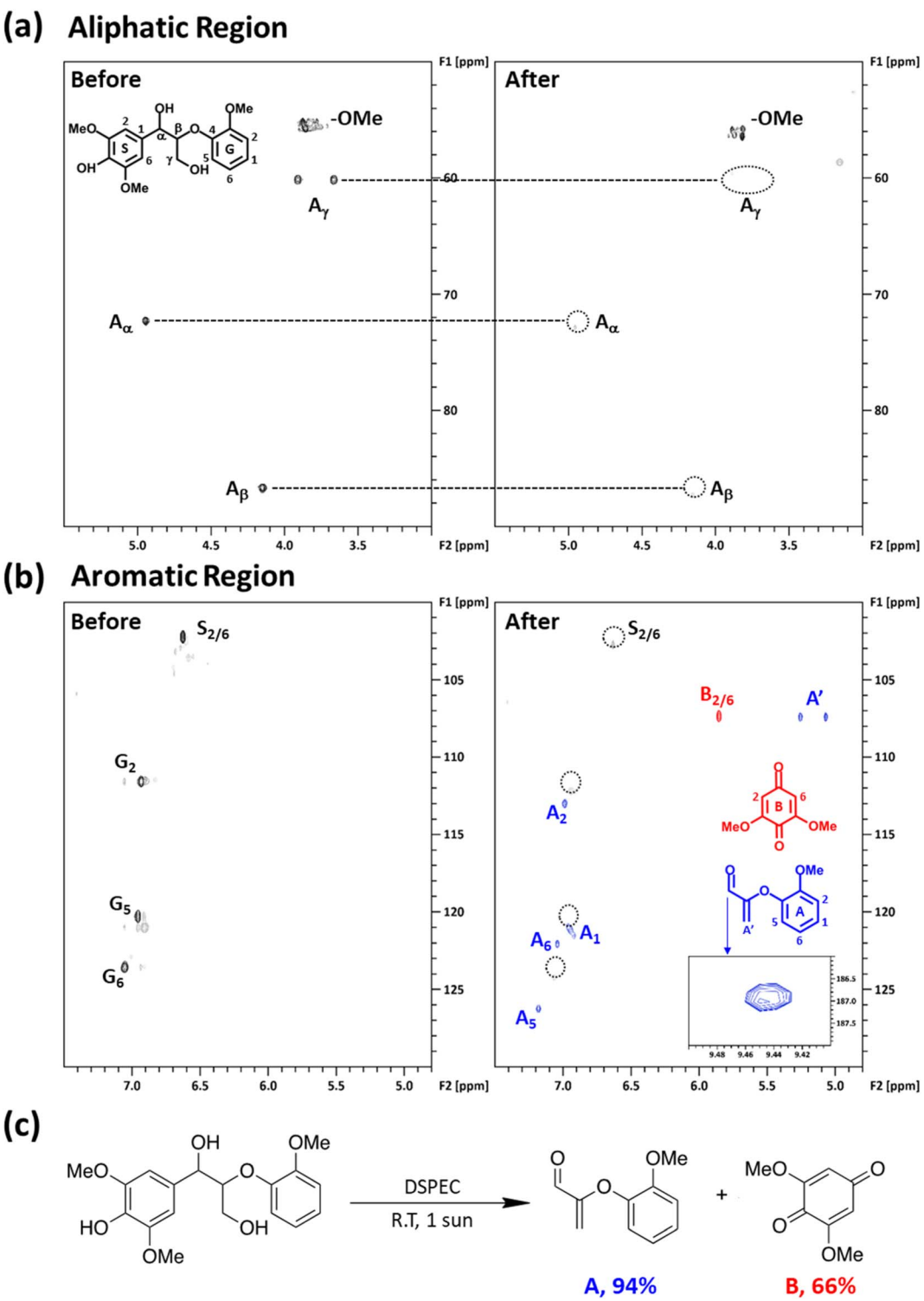

Fig. 5 (a) Aliphatic and (b) aromatic region of 2D HSQC NMR spectra of the **LMC** before (left) and after (right) the photoelectrolysis reaction. (c) Photoelectrocatalytic C–C bond cleavage reaction of a phenolic lignin model compound at the FTO/TiO_2/DPTC incorporating **KABNO** at room temperature. The yields for **A** and **B** were determined by GC-FID analysis of the reaction mixtures relative to dimethyl sulfoxide (DMSO) as an internal standard.

In line with our previous studies, the presence of a chromophore, nitroxyl mediator, and light are all required to perform the effective photocatalytic oxidation of **LMC** at room temperature.[19,48,53] To better understand the products formed during the photocatalytic oxidation of **LMC**, a 24 h continuous illumination experiment with **LMC** and **KABNO** in acetonitrile

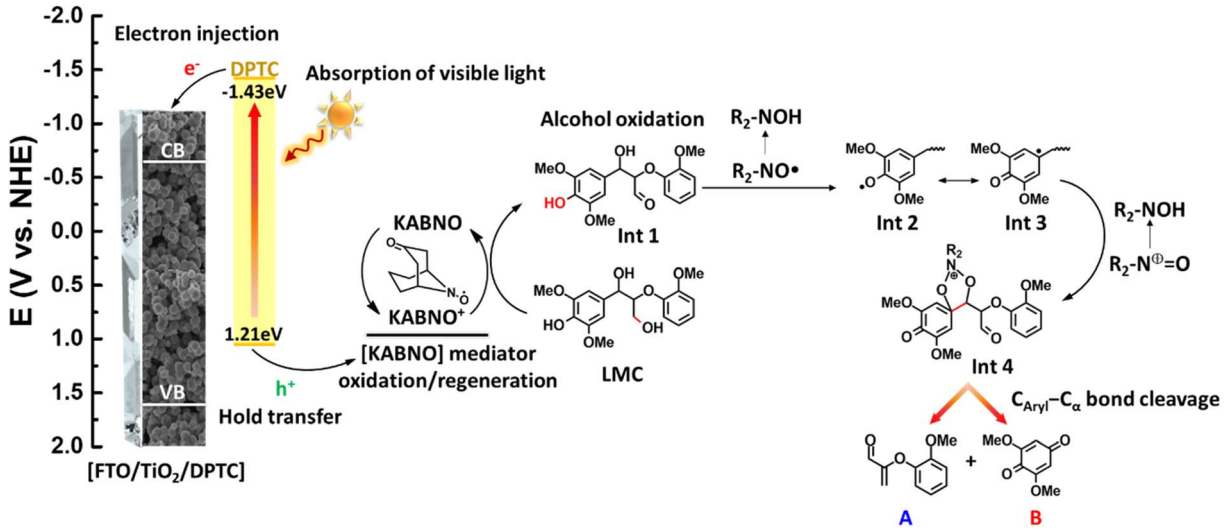

Fig. 6 Proposed mechanism for oxidative C–C bond cleavage to give products **A** and **B** in the DSPEC system by using the FTO/TiO_2/DPTC photoanode and **KABNO** ($R_2NO^{\bullet}$) in the presence of **LMC**.

with 0.1 M $TABPF_6$ was performed. The photocatalytic conversion products were identified using GC-MS and NMR analyses. Cleavage products 2-(2-methoxyphenoxy)acrylaldehyde **A** and 2,6-dimethoxy-1,4-benzoquinone **B** were obtained after the 24 h reaction at room temperature based on the results of GC-MS analysis (Fig. S6†) and ^1H and ^{13}C NMR (Fig. S7†). These products were further confirmed with two-dimensional ^1H–^{13}C heteronuclear single quantum coherence (2D-HSQC) NMR analysis (Fig. 5a and b). In the aliphatic region, the β-aryl ether linkage of **LMC** was identified at δ_C/δ_H 72.27/4.94 ppm (A_α), δ_C/δ_H 86.66/4.15 ppm (A_β), and δ_C/δ_H 60.14/3.91–3.67 ppm (A_γ). These peaks significantly decreased after the 24 h illumination. This observation indicated C–C and/or C–O bond cleavage of the β-aryl ether linkage of **LMC**. For further elucidation of the degradation of **LMC**, the chemical shifts in the aromatic region were identified. The chemical shifts of G_2 (δ_C/δ_H 111.57/6.93 ppm), G_5 (δ_C/δ_H 120.27/6.95 ppm), G_6 (δ_C/δ_H 123.49/7.05 ppm), and $S_{2/6}$ (δ_C/δ_H 102.23/6.62 ppm) were observed with the original **LMC** prior to illumination. However, after the reaction, most of these chemical shifts were not detected. Instead, new chemical shifts from the cleavage products **A** and **B** appeared at A_1 (δ_C/δ_H 121.09/6.95 ppm), A_2 (δ_C/δ_H 112.93/6.99 ppm), A_5 (δ_C/δ_H 126.24/7.18 ppm), A_6 (δ_C/δ_H 122.05/7.04 ppm), A′ ($\delta_C/\delta_{H1}/\delta_{H2}$ 107.34/5.26/5.07 ppm), $B_{2/6}$ (δ_C/δ_H 107.34/5.85 ppm), and the aldehyde peak (δ_C/δ_H 186.91/9.44 ppm). The characteristic signals of **A** and **B** are consistent with our previous report.[52] The yields of products **A** and **B** were quantitatively monitored by GC-FID with DMSO as an internal standard (Fig. S8†). As Fig. 5c presents, after 24 h illumination at room temperature, yields of 94% for **A** and 66% for **B** were obtained. This result is consistent with our previous study where, under aerobic conditions, product **B** could be further oxidized by the oxoammonium form of **KABNO**$^+$ which decreased the measured yield.[52] The trace amount of oxidized **LMC** (1-(4-hydroxy-3,5-dimethoxyphenyl)-2-(2-methoxyphenoxy)propane-1-one) was also observed at δ_C/δ_H 106.48/7.41 ppm (oxidized $S_{2/6}$) and δ_C/δ_H 84.35/5.35 ppm (shifted A_β due to the oxidized OH) as shown in the inset in Fig. S9.† Thus, the above NMR and GC characterizations of the cleavage products after illumination give strong evidence for the selective C_{aryl}–C_α bond cleavage of **LMC**. We were unable to conduct recyclability tests on the same FTO/TiO_2/DPTC photoanode after reaction due to the degradation of the **DPTC** dye at the TiO_2 interface.

Based on the proposed mechanism presented for C_{aryl}–C_α cleavage in aryl ether linkages of a phenolic **LMC** in a related DSPEC system,[43] Fig. 6 illustrates the possible mechanism using the **DPTC**-sensitized photoanode and **KABNO** in the presence of **LMC** at room temperature under 1 sun illumination. The brief overall sequence is as follow: (1) the **DPTC** deposited on the surface of photoanode forms an excited-state **DPTC***, which is sufficiently reducing to sensitize the TiO_2 surface after absorption of visible light; (2) electron injection from **DPTC*** to the conduction band of TiO_2 yields **DPTC**$^+$ and TiO_2 (e^-); (3) **DPTC**$^+$ oxidizes **KABNO** (R_2-$NO^{\bullet}$) to form **KABNO**$^+$ (R_2-N^+ = O) and reform the ground state **DPTC**; (4) one equivalent of **KABNO**$^+$ preferentially oxidizes the primary alcohol (C_γ–OH) of **LMC** to give **Int 1** which leads to the formation of product **B**; (5) abstraction of the phenolic hydrogen atom by R_2-$NO^{\bullet}$ gives the possible **LMC** intermediate radical resonance structures **Int 2** and **Int 3**; (6) reaction of intermediate **Int 3** with an additional equivalent of **KABNO** and **KABNO**$^+$ would then result in the formation of pentacyclic intermediate **Int 4**; (7) dissociation of **Int 4** with the consumption of 1 equivalent of **KABNO**$^+$ and reformation of **KABNO** results in C_{aryl}–C_α cleavage and formation of products **A** and **B**.

Conclusion

Organic dyes have been widely used in dye-sensitized solar cells as an alternative to transition metal complex chromophores. This study confirmed visible light-driven chemoselective C_{aryl}–

C_α bond cleavage in a phenolic **LMC** at room temperature by incorporating the bicyclic nitroxyl mediator **KABNO** and D–π–A type organic dye (**DPTC**). We investigated intermolecular charge transfer between **KABNO** and **DPTC** in solution and at the interface of FTO/TiO_2. The FTO/TiO_2/DPTC photoanode generates significant photocurrent density in the presence of **KABNO** and **LMC** under visible light illumination in acetonitrile electrolyte. This D–π–A type organic dye-based photoelectrochemical process with **KABNO** requires lower applied bias compared to related electrochemical or electrocatalytic approaches and this avoids overoxidation or uncontrolled degradation of the **LMC**. As a result, **LMC** was selectively oxidized in the DSPEC. We anticipate that this system can be further improved and adapted by considering the use of other organic dyes and by tuning the relative redox levels of the various components in the DSPEC. Future work will focus on the preparation of more efficient and chemically stable donor-linker-acceptor components and modifying the dye structure to better match its redox potential to that of the nitroxyl mediator.

Author contributions

S. K., and H. C. K. performed experiments and contributed equally to this project. G. L., and J.-J. L. conceived the idea and provided overall supervision. C. C., S. L., K. Y., and U. K. W. contributed to data acquisition and analysis. W. Z., C. G. Y., and B. D. S. added conceptual contributions and edited the manuscript.

Conflicts of interest

The authors declare no competing financial interest.

Acknowledgements

This work is supported in part by an award from the USDA National Institute of Food and Agriculture, McIntire Stennis project (No. 1026335) and the NYS Department of Economic Development (DED) through the Syracuse Center of Excellence in Environmental and Energy Systems (No. C200183). W. Z. acknowledges support from NSF CAREER grant (Award Number CHE-1944978) and NSF IUCRC Phase I grant (Award Number: 2052611). B. D. S. thanks the Welch Foundation for support of this work through award number P-2044-20200401. J.-J. Lee acknowledge the financial support by the Korean National Research Foundation, funded by the Ministry of Science, ICT & Future Planning (NRF-2021R1A2C2094554).

References

1 S. Li, K. Davis and G. Leem, *ACS Symp. Ser. Am. Chem. Soc.*, 2021, **1377**, 97–121.
2 C. S. Lancefield, L. W. Teunissen, B. M. Weckhuysen and P. C. A. Bruijnincx, *Green Chem.*, 2018, **20**, 3214–3221.
3 C. Díaz-Urrutia, B. Sedai, K. C. Leckett, R. T. Baker and S. K. Hanson, *ACS Sustainable Chem. Eng.*, 2016, **4**, 6244–6251.
4 W. D. do Pim, F. G. Mendonça, G. Brunet, G. A. Facey, F. Chevallier, C. Bucher, R. T. Baker and M. Murugesu, *ACS Appl. Mater. Interfaces*, 2021, **13**, 688–695.
5 L. Dong, L. Lin, X. Han, X. Si, X. Liu, Y. Guo, F. Lu, S. Rudić, S. F. Parker, S. Yang and Y. Wang, *Chem*, 2019, **5**, 1521–1536.
6 M. Wang, J. Lu, X. Zhang, L. Li, H. Li, N. Luo and F. Wang, *ACS Catal.*, 2016, **6**, 6086–6090.
7 L. Ma, H. Zhou, X. Kong, Z. Li and H. Duan, *ACS Sustainable Chem. Eng.*, 2021, **9**, 1932–1940.
8 H. Liu, H. Li, J. Lu, S. Zeng, M. Wang, N. Luo, S. Xu and F. Wang, *ACS Catal.*, 2018, **8**, 4761–4771.
9 Q. Zhang, N. K. Gupta, M. Rose, X. Gu, P. W. Menezes and Z. Chen, *Chem. Catal.*, 2023, **3**, 100470.
10 J. Wang, Y. Deng, Z. Ma, Y. Wang, S. Zhang and L. Yan, *Green Chem.*, 2021, **23**, 5120–5128.
11 S. Trano, F. Corsini, G. Pascuzzi, E. Giove, L. Fagiolari, J. Amici, C. Francia, S. Turri, S. Bodoardo, G. Griffini and F. Bella, *ChemSusChem*, 2022, **15**, e202200294.
12 J. L. Espinoza-Acosta, P. I. Torres-Chávez, J. L. Olmedo-Martínez, A. Vega-Rios, S. Flores-Gallardo and E. A. Zaragoza-Contreras, *J. Energy Chem.*, 2018, **27**, 1422–1438.
13 A. Khan, V. Nair, J. C. Colmenares and R. Gläser, *Top. Curr. Chem.*, 2018, **376**, 20.
14 S. K. Hanson, R. Wu and L. A. P. Silks, *Angew. Chem., Int. Ed.*, 2012, **51**, 3410–3413.
15 T. vom Stein, T. den Hartog, J. Buendia, S. Stoychev, J. Mottweiler, C. Bolm, J. Klankermayer and W. Leitner, *Angew. Chem., Int. Ed.*, 2015, **54**, 5859–5863.
16 S. Gazi, W. K. Hung Ng, R. Ganguly, A. M. Putra Moeljadi, H. Hirao and H. S. Soo, *Chem. Sci.*, 2015, **6**, 7130–7142.
17 G. Zhang, B. L. Scott, R. Wu, L. A. P. Silks and S. K. Hanson, *Inorg. Chem.*, 2012, **51**, 7354–7361.
18 L. J. Mitchell and C. J. Moody, *J. Org. Chem.*, 2014, **79**, 11091–11100.
19 S. Li, Z.-J. Li, H. Yu, M. R. Sytu, Y. Wang, D. Beeri, W. Zheng, B. D. Sherman, C. G. Yoo and G. Leem, *ACS Energy Lett.*, 2020, **5**, 777–784.
20 G. Leem, B. D. Sherman and K. S. Schanze, *Nano Convergence*, 2017, **4**, 37.
21 B. D. Sherman, M. V. Sheridan, K.-R. Wee, S. L. Marquard, D. Wang, L. Alibabaei, D. L. Ashford and T. J. Meyer, *J. Am. Chem. Soc.*, 2016, **138**, 16745–16753.
22 G. Leem, B. D. Sherman, A. J. Burnett, Z. A. Morseth, K.-R. Wee, J. M. Papanikolas, T. J. Meyer and K. S. Schanze, *ACS Energy Lett.*, 2016, **1**, 339–343.
23 D. F. Bruggeman, T. M. A. Bakker, S. Mathew and J. N. H. Reek, *Chem. - Eur. J.*, 2021, **27**, 218–221.
24 S. Yun, N. Vlachopoulos, A. Qurashi, S. Ahmad and A. Hagfeldt, *Chem. Soc. Rev.*, 2019, **48**, 3705–3722.
25 S. Zhang, H. Ye, J. Hua and H. Tian, *EnergyChem*, 2019, **1**, 100015.
26 Y. Ooyama and Y. Harima, *ChemPhysChem*, 2012, **13**, 4032–4080.

27 M. Liang and J. Chen, *Chem. Soc. Rev.*, 2013, **42**, 3453–3488.
28 Z. Fang, J. E. Jackson and E. L. Hegg, *ACS Sustainable Chem. Eng.*, 2022, **10**, 7545–7552.
29 X. Du, H. Zhang, K. P. Sullivan, P. Gogoi and Y. Deng, *ChemSusChem*, 2020, **13**, 4318–4343.
30 M. Garedew, D. Young-Farhat, S. Bhatia, P. Hao, J. E. Jackson and C. M. Saffron, *Sustainable Energy Fuels*, 2020, **4**, 1340–1350.
31 F. Wang and S. S. Stahl, *Acc. Chem. Res.*, 2020, **53**, 561–574.
32 M. Rafiee, M. Alherech, S. D. Karlen and S. S. Stahl, *J. Am. Chem. Soc.*, 2019, **141**, 15266–15276.
33 I. Bosque, G. Magallanes, M. Rigoulet, M. D. Kärkäs and C. R. J. Stephenson, *ACS Cent. Sci.*, 2017, **3**, 621–628.
34 A. Rahimi, A. Azarpira, H. Kim, J. Ralph and S. S. Stahl, *J. Am. Chem. Soc.*, 2013, **135**, 6415–6418.
35 M. Shibuya, M. Tomizawa, I. Suzuki and Y. Iwabuchi, *J. Am. Chem. Soc.*, 2006, **128**, 8412–8413.
36 S. Hamada, T. Furuta, Y. Wada and T. Kawabata, Chemoselective Oxidation by Electronically Tuned Nitroxyl Radical Catalysts, *Angew. Chem., Int. Ed.*, 2013, **52**, 8093–8097.
37 M. Rafiee, K. C. Miles and S. S. Stahl, *J. Am. Chem. Soc.*, 2015, **137**, 14751–14757.
38 L. N. Grigor'eva, A. Y. Tikhonov, K. A. Lomanovich and D. G. Mazhukin, *Molecules*, 2021, **26**, 3050.
39 D. P. Hagberg, T. Marinado, K. M. Karlsson, K. Nonomura, P. Qin, G. Boschloo, T. Brinck, A. Hagfeldt and L. Sun, *J. Org. Chem.*, 2007, **72**, 9550–9556.
40 M. B. Lauber and S. S. Stahl, *ACS Catal.*, 2013, **3**, 2612–2616.
41 G. Leem, Z. A. Morseth, E. Puodziukynaite, J. Jiang, Z. Fang, A. T. Gilligan, J. R. Reynolds, J. M. Papanikolas and K. S. Schanze, *J. Phys. Chem. C*, 2014, **118**, 28535–28541.
42 G. Leem, Z. A. Morseth, K.-R. Wee, J. Jiang, M. K. Brennaman, J. M. Papanikolas and K. S. Schanze, *Chem.–Asian J.*, 2016, **11**, 1257–1267.
43 N. C. D. Nath, S. Sarker, A. J. Saleh Ahammad and J.-J. Lee, *Phys. Chem. Chem. Phys.*, 2012, **14**, 4333.
44 N. C. D. Nath, J. C. Kim, K. P. Kim, S. Yim and J.-J. Lee, *J. Mater. Chem. A.*, 2013, **1**, 13439.
45 G. I. Lee, N. C. D. Nath, S. Sarker, W. H. Shin, A. J. S. Ahammad, J. K. Kang and J.-J. Lee, *Phys. Chem. Chem. Phys.*, 2012, **14**, 5255.
46 A. Venkateswararao, K. R. J. Thomas, C.-P. Lee, C.-T. Li and K.-C. Ho, *ACS Appl. Mater. Interfaces*, 2014, **6**, 2528–2539.
47 A. Tiwari and U. Pal, *Int. J. Hydrogen Energy*, 2015, **40**, 9069–9079.
48 S. Li, E. W. Shuler, D. Willinger, H. T. Nguyen, S. Kim, H. C. Kang, J.-J. Lee, W. Zheng, C. G. Yoo, B. D. Sherman and G. Leem, *ACS Appl. Mater. Interfaces*, 2022, **14**, 22799–22809.
49 H. Jiang, Y. Cheng, Z. Wang, Z. Bai, Y. Tang, Y. Sun, P. Wan and Y. Chen, *J. Electrochem. Soc.*, 2021, **168**, 016504.
50 J. E. Nutting, M. Rafiee and S. S. Stahl, *Chem. Rev.*, 2018, **118**, 4834–4885.
51 C. Yang, S. Maldonado and C. R. J. Stephenson, *ACS Catal.*, 2021, **11**, 10104–10114.
52 S. Li, S. Kim, A. H. Davis, J. Zhuang, E. W. Shuler, D. Willinger, J.-J. Lee, W. Zheng, B. D. Sherman, C. G. Yoo and G. Leem, *ACS Catal.*, 2021, **11**, 3771–3781.
53 S. Li, S. Park, B. D. Sherman, C. G. Yoo and G. Leem, *Chem. Commun.*, 2023, **59**, 401–413.

